applied sciences

MDPI

Article

Research on Head Pursuit Interception Strategy for Hypersonic Target

Zhihan Li and Ying Nan *

Academy of Astronautics, Nanjing University of Aeronautics and Astronautics, Nanjing 210016, China; lzh_astro@nuaa.edu.cn
* Correspondence: nanying@nuaa.edu.cn

Abstract: In the wake of countries competing to develop high-efficiency offensive weapons, high-precision systems have also developed. Due to the high speed and high maneuverability of hypersonic targets, it is always difficult to meet the accuracy and rapidity requirements by using the traditional interception mode. In order to improve the accuracy of the hypersonic target interception, a head pursuit guidance strategy is developed for hypersonic target interception in this study. Firstly, a dynamic model is established by analyzing the relative motion between the interceptor and the target, which needs to place the low-speed interceptor before the high-speed target. Subsequently, a head pursuit interception guidance strategy is presented, which controls the interceptor flight trajectory by controlling its normal acceleration to achieve a successful interception target. Finally, for the maneuvering and non-maneuvering targets, the dynamic characteristics of interceptor are analyzed, respectively, and full trajectory dynamic simulations under different conditions for the hypersonic target interception are worked out to illustrate the feasibility and robustness of the proposed guidance strategy.

Keywords: hypersonic target; maneuvering; head pursuit; full trajectory; guidance strategy

Citation: Li, Z.; Nan, Y. Research on Head Pursuit Interception Strategy for Hypersonic Target. *Appl. Sci.* **2023**, *13*, 4772. https://doi.org/10.3390/app13084772

Academic Editors: Xiangwei Bu and Zhonghua Wu

Received: 13 March 2023
Revised: 9 April 2023
Accepted: 10 April 2023
Published: 10 April 2023

1. Introduction

Currently, the main objects of an interception system are ballistic missiles and various homing missiles. The exoatmospheric midcourse interception system, various endoatmospheric terminal interception systems, and initial interception systems for such objects are currently in the stage of deployment or are about to be deployed. Various countries have introduced various penetration means for targeted research, which are in response to the increasingly severe threats of ballistic missiles.

Based on the characteristics of the existing antimissile systems, a hypersonic aircraft is studied and used as an effective penetration means. Unlike ballistic missiles, hypersonic aircrafts adopt the boost glide or cruise mode, giving them a faster response, better penetration effect, higher strike accuracy, and greater damage power. The interception of hypersonic targets requires a higher interception range and accurate interceptor guidance. However, it is difficult to meet the guidance accuracy requirement or the cost is too high to intercept hypersonic targets using traditional methods.

The Mach number of a hypersonic target is usually above 6. When the interceptor intercepts the target head-on, the relative velocity of the interceptor and the target will be very large. Once the target maneuvers and deviates from the predicted trajectory, the interceptor needs to deal with it in a short time. However, it is difficult to control the interceptor, thus failing to meet the interception accuracy requirements and easily causing a miss; if the tail pursuit method is used for interception, the interceptor speed is required to be higher than the target speed. This method also leads to difficulties in controlling the interception accuracy and also puts forward higher performance requirements for the interceptor.

In order to overcome these difficulties, Golan O. M. put forward a head pursuit interception idea, that is, the interceptor is placed on the predicted flight trajectory in front of the target by maneuvering, and the flight direction is consistent with it [1,2]. Because the interceptor has a lower flight speed, the target approaches the interceptor, thus achieving the interception. This interception mode converts an interceptor speed greater than the target speed into an interceptor speed less than the target speed and reduces the energy demand of the interceptor and thus reduces the control difficulty and interception cost. To research the quality of the air-to-air interceptor guidance strategy, it is necessary to research the head pursuit interception mode guidance strategy. For the proportional navigation (PN) guidance law and its derived modified guidance law and three-dimensional guidance law, their basic ideas are to apply the control force in the direction of reducing the line-of-sight angular rate. The proportional navigation guidance methods have some theoretical defects when dealing with such objects. They cannot guarantee the stability of line-of-sight in the terminal guidance phase, which is equivalent to simple proportional feedback. Therefore, the line-of-sight angle at the end may diverge, and the miss distance will be too large.

Zhang established a three-dimensional model of face-to-face interception in which the interceptor and the target move in opposite directions, which is quite different from head pursuit interception [3]. Zhou designed a three-dimensional guidance law based on proportional navigation, but its guidance law is based on ballistic linearization, and the limitation of proportional navigation is great [4]. Zhao designed the guidance law based on the quasiparallel approach principle [5,6]. His guidance law only needed to keep the line-of-sight angle as a constant and did not require the interceptor to be in the same direction as the target velocity. Therefore, the guidance law was not only applicable to head pursuit interception. However, the guidance law needed a large overload to intercept maneuvering targets, and the angular velocity of the line of sight at the end of the guidance easily diverged. Wang used the auxiliary circle design guidance law algorithm to make the interceptor intercept along the auxiliary circle [7], and Guan applied the neural network PID control to the hypersonic vehicle [8]. These two methods were simple and effective but did not have good adaptability to target maneuvering.

Ratnoo used the method of integrated guidance to meet different terminal attack angles through the combined change of the navigation coefficient of the proportional navigation guidance to pursue stationary or nonstationary targets [9,10]. Offset proportional guidance was combined with convex optimization to solve the rocket vertical return fixed point soft landing guidance problem with landing angle, landing speed, and thrust range constraints by An [11]. In order to expand the acquisition area of the classical proportional navigation guidance law and improve its utilization ability for missile maneuver, Wang designed a time-varying guidance coefficient, so that the proposed guidance scheme could integrate the advantages of proportional and inverse proportional guidance laws [12]. Yan proposed a three-dimensional joint offset proportional guidance law, which used the time-varying offset angular rate and time-varying proportional coefficient, combined with the advantages of forward and reverse orbit interception modes [13]. Mu studied the guidance law combining offset proportional guidance and sliding mode control [14,15].

The application of sliding mode control in a non-linear model has been widely developed in recent years. Using sliding mode control for multi-constraint guidance had become a research hotspot [16–19]. Si and Yang selected a nonsingular fast terminal sliding mode surface with an attack angle constraint and, combined with dynamic surface control, a new guidance law was proposed to make the attack angle and attack angle rate converge in a finite time [20,21]. Furthermore, You and Li applied sliding mode control to cooperative guidance and designed a dual cooperative guidance law from the line-of-sight direction and the line-of-sight normal direction so as to realize the simultaneous interception of multiple missiles at the desired attack angle [22,23]. For the interception of maneuvering targets, Lyu proposed a maneuvering target pursuit guidance law with line-of-sight angle constraints to meet the requirements of attacking maneuvering targets at the desired line-of-sight angle [24]. Harl deduced the line-of-sight angle polynomial, which took the

horizontal position of the missile as the independent variable and met the constraints of the attack time and the attack angle [25]. The guidance command was designed based on second-order sliding mode theory to realize the simultaneous control of the attack time and attack angle. However, the designed Los polynomial needed the missile position at each time, and the measurement accuracy of the position information was too high in practical application.

For the interception of hypersonic targets, the longitudinal motion is determined only by the magnitude of the pitch angle, while the lateral motion is determined only by the positive and negative of the pitch angle. Therefore, the lateral and longitudinal motion can be studied, respectively. Zhang studied the trajectory planning of the interceptor for a hypersonic target, comprehensively considered three factors—terminal speed, terminal miss distance, and aerodynamic heating—and solved the trajectory using a particle swarm optimization algorithm [26]. Shaferman proposed an optimal guidance law for intercepting hypersonic targets based on linear quadratic theory, which ensures that multiple missiles have a favorable geometric situation relative to maneuvering targets during interception [27]. Shima proposed a cooperative guidance law based on the linear quadratic optimal control method, which makes the change rate of relative angle of view between adjacent missiles tend to zero when intercepting hypersonic maneuvering targets [28]. Shaferman studied the guidance problem of multiple interceptors intercepting hypersonic maneuvering targets from different directions based on cooperative differential games [29]. Gaudet proposed a new guidance law based on reinforcement learning [30]. This guidance form does not need distance estimation but only needs to observe the line-of-sight angle and its change rate of the seeker, so it is suitable for a passive seeker.

In this paper, a sliding mode guidance law is designed by establishing a head pursuit interception model, according to the restrictions of head pursuit interception and combining the advantages of proportional navigation, using the adaptive characteristics of variable structure control to against jamming. This guidance law adopts the idea of controlling the interceptor to be proportional to the altitude angle of the target. The low-speed interceptor is controlled before the high-speed target from beginning to end and has good robustness. Moreover, the target is usually maneuverable in the interception process according to the actual situation. In this paper, simulation is carried out under the condition of a 5 g maneuvering target to verify the accuracy of the guidance law.

The guidance strategy designed in this paper can effectively deal with the adverse effects caused by the escape mode of hypersonic targets with large maneuvers and the dynamic characteristics of the missile body and achieve good guidance quality.

2. Model of Interceptor

2.1. Aerodynamic Characteristics of Interceptor

In current research on the guidance law, interceptors fly mainly at a constant speed, but in the actual interception process, interceptors are easily affected by external disturbances, thus affecting the guidance quality. Therefore, it is necessary to further study the guidance law in the case of external interference. In recent research on the aerodynamic characteristics of missiles, researchers analyzed the aerodynamic characteristics of different types of missiles and obtained the variation trend of lift and drag at different velocities and angles of attack by numerical calculation [31–33].

The aerodynamic layout of a missile directly determines its overall aerodynamic characteristics. In this section, the geometric shape model of the interceptor is established. After grid processing, the numerical calculation of aerodynamic characteristics is carried out to obtain the aerodynamic force and aerodynamic coefficient under different Mach numbers and different angles of attack and side-slip, and then it is substituted into the subsequent designed guidance law to simulate the interception process.

Figure 1 shows the 3D interceptor model. This interceptor is made up of a missile body and rudder wings. Rudder wings are distributed in a cross shape at the tail and are

used to change the attitude of the interceptor. The interceptor parameters are shown in Table 1.

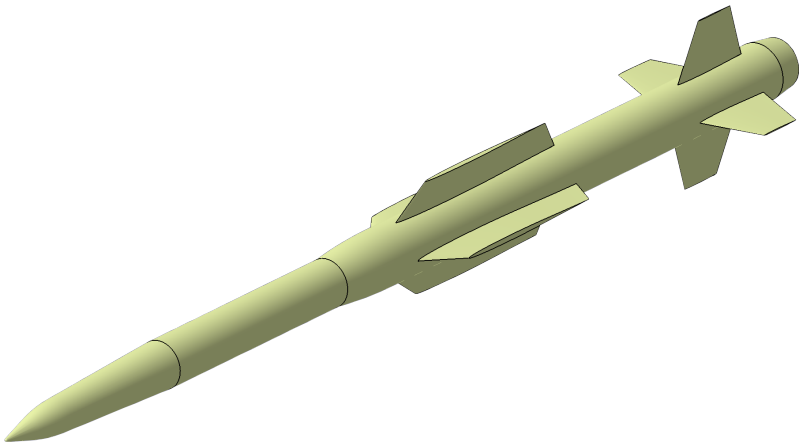

Figure 1. Model of interceptor.

Table 1. Parameters of Interceptor.

Parameters	Length/m	Diameter/m	Wing Type	Takeoff Weight/kg
Datas	5.2	0.28	Cruciform	300

The external flow field of the interceptor model is established and meshed. Based on the flow field domain of the grid, the aerodynamic characteristics of the interceptor are calculated by the fluid calculation method, and the aerodynamic coefficients of the interceptor are obtained [34], as shown in Figures 2–4.

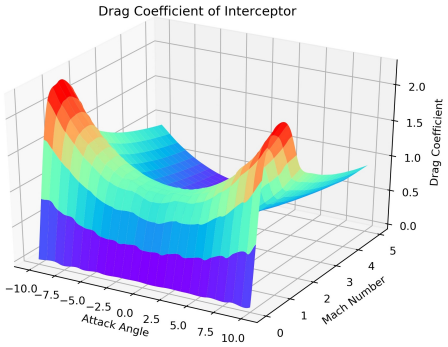

Figure 2. Drag coefficient.

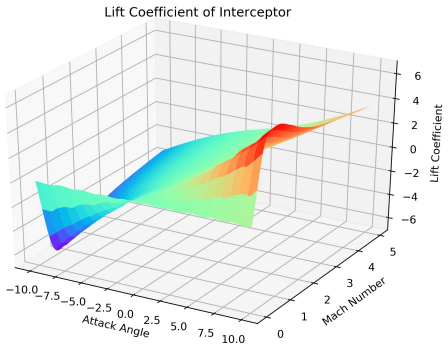

Figure 3. Lift coefficient.

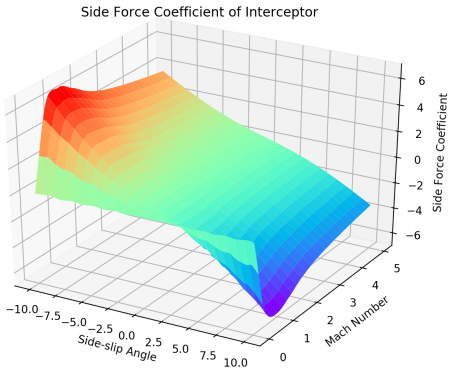

Figure 4. Side force coefficient.

2.2. Model of Head Pursuit Interception

The study of guidance trajectory is based on the laws of classical mechanics. In the preliminary design phase of a guidance system, kinematics analysis methods are generally used in order to simplify the research. The relative motion equation describes the relative motion of the interceptor and target. The establishment of the relative motion equation is the basis of a guidance trajectory kinematics analysis method.

In the interception process controlled by a direct driving force, it is assumed that the maneuvering acceleration vectors of the interceptor and the target are perpendicular to their velocity vectors in order to simplify the analysis process of the problem, that is, the maneuvering acceleration vectors only change their velocity directions without changing the size of the velocity scalars. The x-direction of this coordinate system coincides with the velocity vector of the missile center of mass and has the same direction. The y-direction is perpendicular to the velocity vector and is in the vertical plane containing the y-axis. The z-direction is determined by the right-hand rule.

The ballistic (trajectory) coordinate system is a dynamic coordinate system fixed to the velocity vector **V**, with the origin fixed to the missile body and taken at the center of mass of the missile. The coordinate system moves with the motion of missiles and is often used to study the motion characteristics of missile centroids.

Figure 5 shows the relative motion of the missile and the target. T and M represent the target and interceptor, respectively. $OXYZ$ represents the inertial coordinate system, and $OX_lY_lZ_l$ represents the line-of-sight coordinate system. R is the range of them. V_T and V_M represent velocity vectors, and A_T and A_M represent acceleration vectors. q_H and q_L represent the pitch angle and yaw angle of the line-of-sight. η_{TH} and η_{TL} represent the angle between V_T and the line-of-sight, which are defined as the attitude angle of the target. η_{MH} and η_{ML} represent the angle between V_M and the line-of-sight, which are defined as the attitude angle of the interceptor.

In the interception process studied in this paper, the target performs a maneuvering flight. According to the classification of the maneuver trajectory, typical terminal maneuver modes include the jump–dive maneuver, snake maneuver, pendulum maneuver, and spiral maneuver. The hypersonic target studied in this paper starts the snake maneuver at a certain time, and the maximum maneuver overload is 5 g.

The kinematic equations of the maneuvering target are established in the inertial frame as follows.

$$\begin{cases} \dot{X}_T = V_T \cos\varphi_T \cos\psi_T \\ \dot{Y}_T = V_T \sin\varphi_T \\ \dot{Z}_T = -V_T \sin\varphi_T \cos\psi_T \end{cases} \tag{1}$$

Considering the ballistic frame, the following expressions can be obtained.

$$\begin{cases} \dot{\varphi}_T = \frac{N_{TY}g}{V_T} \\ \dot{\psi}_T = -\frac{N_{TZ}g}{V_T \cos\varphi_T} \end{cases} \tag{2}$$

The kinematic equations of the interceptor are established in the inertial frame as follows.

$$\begin{cases} \dot{X}_M = V_M \cos\varphi_M \cos\psi_M \\ \dot{Y}_M = V_M \sin\varphi_M \\ \dot{Z}_M = -V_M \sin\varphi_M \cos\psi_M \end{cases} \tag{3}$$

Considering the ballistic frame, the following expressions can be obtained.

$$\begin{cases} m\dot{V}_M = P\cos\alpha\cos\beta - X - mg\sin\varphi_M \\ mV_M\dot{\varphi}_M = P\sin\alpha + Y - mg\cos\varphi_M \\ mV_M\dot{\psi}_M = P\cos\alpha\sin\beta - Z \\ \dot{\varphi}_M = \frac{(N_{MY}-\cos\varphi_M)g}{V_M} \\ \dot{\psi}_M = -\frac{N_{MZ}g}{V_M\cos\varphi_M} \end{cases} \tag{4}$$

where P represents the thrust of the interceptor engine; X, Y, and Z represent the aerodynamic drag, lift, and side force of the interceptor, respectively; α and β represent the angle of attack and the angle of side-slip of the interceptor; φ represents the flight-path inclination angle, which is the angle between the velocity vector and the horizontal plane; ψ represents the azimuth angle, which is the angle between the velocity vector and the vertical plane; φ_T and ψ_T represent the flight-pathinclination angle and azimuth angle of the target, respectively; φ_M and ψ_M represent the trajectory inclination angle and azimuth angle of the interceptor, respectively; N_{TY} and N_{TZ} represent the normal overload of the target in the longitudinal and lateral channels, with sizes of A_{TY}/g and A_{TZ}/g, respectively; and N_{MY} and N_{MZ} represent the normal overload of the interceptor in the longitudinal and lateral channels, with sizes of A_{MY}/g and A_{MZ}/g, respectively.

The following matrices are derived through the coordinate system transformation by Equations (6)–(9).

$$\mathbf{T}_L = \begin{bmatrix} \cos q_H \cdot \cos q_L & \sin q_H & -\cos q_H \cdot \sin q_L \\ -\sin q_H \cdot \cos q_L & \cos q_H & \sin q_H \cdot \sin q_L \\ \sin q_L & 0 & \cos q_L \end{bmatrix} \tag{5}$$

$$\mathbf{T}_T = \begin{bmatrix} \cos\varphi_T \cdot \cos\psi_T & \sin\varphi_T & -\cos\varphi_T \cdot \sin\psi_T \\ -\sin\varphi_T \cdot \cos\psi_T & \cos\varphi_T & \sin\varphi_T \cdot \sin\psi_T \\ \sin\psi_T & 0 & \cos\psi_T \end{bmatrix} \tag{6}$$

$$\begin{bmatrix} V_{TLX} \\ V_{TLY} \\ V_{TLZ} \end{bmatrix} = \mathbf{T}_L \cdot {\mathbf{T}_T}^{-1} \cdot \begin{bmatrix} V_T \\ 0 \\ 0 \end{bmatrix} \tag{7}$$

$$\mathbf{T}_M = \begin{bmatrix} \cos\varphi_M \cdot \cos\psi_M & \sin\varphi_M & -\cos\varphi_M \cdot \sin\psi_M \\ -\sin\varphi_M \cdot \cos\psi_M & \cos\varphi_M & \sin\varphi_M \cdot \sin\psi_M \\ \sin\psi_M & 0 & \cos\psi_M \end{bmatrix} \tag{8}$$

$$\begin{bmatrix} V_{MLX} \\ V_{MLY} \\ V_{MLZ} \end{bmatrix} = \mathbf{T}_L \cdot {\mathbf{T}_M}^{-1} \cdot \begin{bmatrix} V_M \\ 0 \\ 0 \end{bmatrix} \tag{9}$$

where $\mathbf{T}_T$ and $\mathbf{T}_M$ represent the transformation matrix from the inertial or earth coordinate system to the ballistic coordinate system of the target and interceptor, respectively. $\mathbf{T}_L$ represents the transformation matrix from the inertial coordinate system to the line-of-sight coordinate system.

Thus, the representation of the relative motion of the interceptor and target can be deduced.

$$\begin{cases} \dot{R} = V_{TLX} - V_{TMX} \\ \dot{q}_H = \frac{V_{TLY} - V_{TMY}}{R} \\ \dot{q}_L = \frac{V_{TLZ} - V_{TMZ}}{R \cos q_H} \end{cases} \tag{10}$$

The requirement of the head pursuit interception mode is to place the interceptor in front of the target, bring the interceptor close to the predicted flight trajectory of the target, and make them move in the same direction. The Mach number of the interceptor should be less than that of the target. The coefficient K is taken as follows:

$$K = \frac{V_M}{V_T} < 1 \tag{11}$$

To intercept a target successfully, the range is limited not only to 0 at the intercept point but also to keep the direction of motion identically. This leads to the following:

$$\lim_{R \to 0} \eta_{MH} = 0 \&\& \lim_{R \to 0} \eta_{ML} = 0 \tag{12}$$

$$\lim_{R \to 0} \eta_{TH} = 0 \&\& \lim_{R \to 0} \eta_{TL} = 0 \tag{13}$$

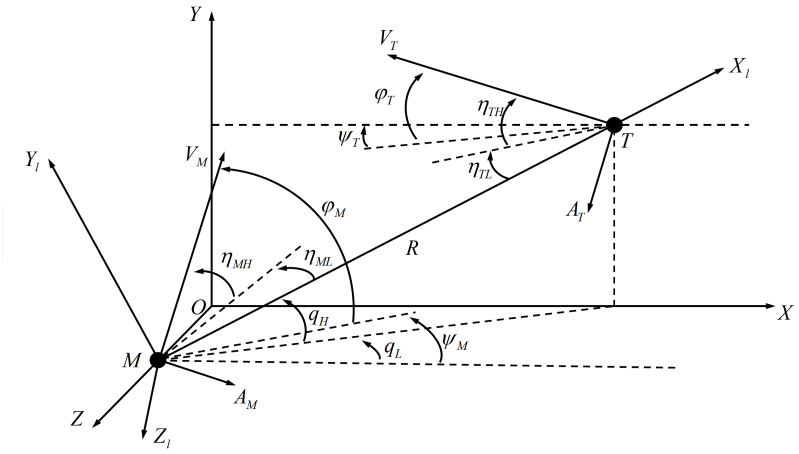

Figure 5. Relative motion of the interceptor and target.

2.3. Simulation Model

To verify the feasibility of the guidance strategy designed in this study, it is necessary to simulate the entire trajectory of the intercept. Considering the convenience of program debugging and the expandability of functions, the simulation system is based on the composition principle of the guidance and control system and is divided into different modules according to physical functions. The simulation model is shown in Figure 6.

As can be seen in Figure 6, the simulation system model includes four modules, namely the target module, interceptor module, relative motion of the interceptor, target module, and guidance module. These four modules are introduced in the following.

(1) Target module

The target module solves the real-time position and velocity information of the target according to the target kinematics model.

(2) Interceptor module

The main function of the interceptor module is to calculate the position, speed, and attitude information of the interceptor at each time according to the input deflection angle of the rudders. It also includes the interpolation calculation of the center of gravity, mass, moment of inertia, aerodynamic force and torque of the missile, and engine thrust.

(3) Relative motion of the interceptor and the target module

This module is used to replace the guidance information calculation function of the seeker and to solve the missile target relative distance and relative distance change rate, line-of-sight angle, and line-of-sight angle rate information according to the speed and position information of the interceptor and the target.

(4) Guidance module

This module includes the seeker, the estimation of target maneuvers, and the generation of guidance instructions. The seeker outputs information on the change rate of the relative distance of the missile target, line-of-sight angle, and line-of-sight angle rate. This information is used as an observation of target maneuver estimation, estimates the acceleration of the target, and outputs it to the guidance instruction formation module to calculate the guidance law.

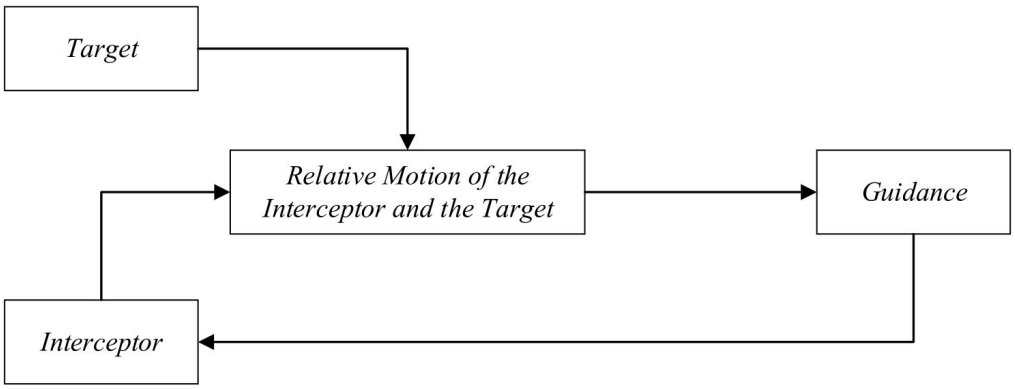

Figure 6. Diagrammatic sketch of side force coefficient.

3. Design of Head Pursuit Interception Guidance Strategy

The missile interception system is a strongly coupled non-linear system. Consider the following non-linear system [35]:

$$\dot{X} = f(X,t) + G_1(X,t)u + G_2(X,t)w \tag{14}$$

where X is the state variable, u is the controlled variable, and w is the uncertainty of the system. Taking the overload N_{MY} and N_{MZ} of the interceptor as the control variables, the guidance strategies of the initial guidance phase, the midcourse guidance phase, and the terminal guidance phase are designed, respectively.

3.1. Design of Initial Guidance Law

In the initial guidance phase, the combination of longitudinal and lateral channel control is used to make the interceptor climb to the predetermined height and direction. To ensure the stability of interceptor flight control loop in large airspace, the controllers of the longitudinal and lateral loop are designed based on the preset turning angle and improved proportional navigation guidance method in the initial phase. The interceptor needs to accelerate to a certain Mach number and meet the condition that the flight-path inclination angle of the interceptor is about 90 degrees at the end. That is, the interceptor turns at a certain angle at the end of the initial guidance, and thus the relationship of the interceptor and target does not need to be considered. The concept of a preset turning point is introduced, and the point is taken as the target in the initial guidance phase. The problem becomes that the interceptor intercepts the air-fixed target at a certain terminal ballistic angle.

The preset turning point coordinates are assumed to be $TP(X_{TP}, Y_{TP}, Z_{TP})$, the initial coordinates of the interceptor are $M(X_{M0}, Y_{M0}, Z_{M0})$, and the initial coordinates of the target are $T(X_{T0}, Y_{T0}, Z_{T0})$.

The key to determining X_{TP} is to find its expression about the initial horizontal distance ΔX of the missile and the target, that is, $X_{TP} = f(\Delta X)$. According to the kinematic relationship, the following equation can be obtained:

$$\Delta X_{\min} < \Delta X - (X_{TP} + V_T t_d) < \Delta X_{\max} \tag{15}$$

where ΔX is the initial horizontal distance between interceptor and target; $\Delta X_{\min}$ is the minimum horizontal distance between the missile and the target at the end of the initial guidance, to ensure that the interceptor in the middle and terminal guidance phase is not exceeded by the target; and $\Delta X_{\max}$ is the maximum horizontal distance between the missile and the target at the end of the initial guidance, to ensure that the terminal guidance phase of the interceptor will not be too long.

When ΔX is certain and within the interception range, there is a feasible range corresponding to X_{TP}. That is, as long as $X_{TP} \in (X_{TP\min}, X_{TP\max})$ is taken, the interceptor can hit the target.

Through several groups of simulations, the corresponding feasible range of X_{TP} under different ΔX and the optimal value X_{TPopt} of the corresponding X_{TP} are determined. Then, the expression of X_{TP} changing with ΔX is fitted according to these data groups, which are shown in Table 2.

Table 2. Values of X_{TP}.

ΔX/km	**200**	**250**	**300**	**350**	**400**
$X_{TP\min}$/km	31.28	32.77	33.67	34.26	34.25
$X_{TP\max}$/km	29.5	30.28	30.56	30.34	29.62
X_{TPopt}/km	29.3	29.3	29.3	29.3	29.3

By fitting the data in Table 2, the expression for X_{TP} can be obtained. Due to the small initial height difference and lateral distance difference between the target and the interceptor compared to the initial horizontal distance, the impact of changing Y_{TP} and Z_{TP} is minimal. Therefore, expressions for Y_{TP} and Z_{TP} can be designed within a reasonable range, all of which are listed as follows.

$$\begin{cases} X_{TP} = -0.0001(X_{T0} - X_{M0})^2 + 0.0606(X_{T0} - X_{M0}) + 21,385 \\ Y_{TP} = Y_{T0} - Y_{M0} \\ Z_{TP} = Z_{m0} + \frac{1}{3}(Z_{T0} - Z_{M0}) \end{cases} \tag{16}$$

According to the three-dimensional proportional navigation guidance method, the longitudinal channel and lateral channel guidance laws of the initial guidance phase are designed as follows.

(1) Longitudinal channel

$$N_{MY} = \frac{k_1 |\dot{R}| \dot{q}_H}{g} \tag{17}$$

(2) Lateral channel

$$N_{MZ} = \frac{k_2 |\dot{R}| \dot{q}_L}{g} \tag{18}$$

where k_1 and k_2 are proportional navigation guidance parameters, which are constants and typically range from 2 to 6.

3.2. Design of Midcourse Guidance Law

The purpose of midcourse guidance is to guide the interceptor to the distance that the terminal guidance seeker can intercept the target and to make the seeker complete the interception of angle and distance. An excellent midcourse guidance law should make the

interceptor work in the best state of its overload performance throughout the midcourse guidance process and make the interceptor lock the target, that is, at the beginning of the terminal guidance phase, the geometric relationship between the interceptor and the target reaches the optimal state.

The guidance method based on impact point prediction estimates the collision position between the interceptor and the target, changes the real target flying at high speed into a false target moving at low speed, fully reduces the demand overload of the interception trajectory, and improves the hit accuracy. It is always used to intercept high-speed targets by head-on interception. The method of head pursuit interception in this paper learns from the idea of the traditional guidance method of impact point prediction, takes this point as the fixed point, and designs the midcourse guidance strategy based on optimal control theory.

(1) Longitudinal channel

The longitudinal channel guidance strategy must guide the interceptor to the same flight altitude as the target and maintain this altitude until it reaches the predicted impact point. Based on the sliding mode control theory, a longitudinal channel midcourse guidance law is designed. The difference between the interceptor altitude and target altitude is assumed to be e, and the altitude command signal is H_c.

$$e = H_c - Y_M \tag{19}$$

The derivative is as follows.

$$\dot{e} = \dot{H}_c - \dot{Y}_M \tag{20}$$

The sliding mode surface is designed as follows.

$$S_{H\_mid} = ce + \dot{e} \tag{21}$$

where c is a sliding mode guidance parameter, which is a constant greater than 0.

The reaching law is designed as follows.

$$\dot{S}_{H\_mid} = -k_3 \mathrm{sgn}(S_{H\_mid}) - \varepsilon S_{H\_mid} \tag{22}$$

where k_3 and ε are sliding mode guidance parameters, which are constants and typically range from 0 to 1.

According to the Lyapunov stability criterion, the function is defined:

$$V = \frac{1}{2} S_{H\_mid}^2 \tag{23}$$

Then,

$$\begin{aligned} \dot{V} &= S_{H\_mid} \dot{S}_{H\_mid} \\ &= S_{H\_mid}(-k_3 \mathrm{sgn}(S_{H\_mid}) - \varepsilon S_{H\_mid}) \\ &= -k_3 |S_{H\_mid}| - \varepsilon S_{H\_mid}^2 < 0 \end{aligned} \tag{24}$$

According to Equation (24), the designed sliding mode surface meets the Lyapunov stability theorem, and the feasibility of the designed guidance law is verified theoretically.

The following equation can be obtained by substituting the derivative of the surface into Equation (22):

$$c\dot{e} + \left(\ddot{H}_c - \ddot{Y}_M\right) = -\varepsilon \mathrm{sgn}(S_{H\_mid}) - k_3 S_{H\_mid} \tag{25}$$

Then,

$$\ddot{Y}_M = c\dot{e} + \ddot{H}_c + \varepsilon \mathrm{sgn}(S_{H\_mid}) + k_3 S_{H\_mid} \tag{26}$$

From Equation (4),

$$\dot{\varphi}_M = \frac{(N_{MY} - \cos\varphi_M)g}{V_M} \tag{27}$$

$$\ddot{Y}_M = \dot{V}_M \sin\varphi_M + \dot{\varphi}_M V_M \cos\varphi_M \tag{28}$$

The longitudinal channel midcourse guidance law can be obtained.

$$N_{MY} = \frac{c\dot{e} + \ddot{H}_c + \varepsilon \mathrm{sgn}(S_{H\_mid}) + k_3 S_{H\_mid} + g\cos^2\varphi_M - \dot{V}_M \sin\varphi_M}{g\cos\varphi_M} \tag{29}$$

(2) Lateral channel

According to Equation (10), the following is obtained.

$$\ddot{q}_L = \left(\frac{\dot{V}_{ML}}{V_{ML}} - \frac{2\dot{R}_L}{R_L}\right)\dot{q}_L + \frac{\dot{R}_L}{R_L}\dot{\psi}_M \tag{30}$$

The terminal constraint commands the line-of-sight angle equal to the required velocity inclination angle, and the line-of-sight angular velocity is zero.

$$\begin{cases} q_L\left(t_f\right) = \psi_{Mf} \\ \dot{q}_L\left(t_f\right) = 0 \end{cases} \tag{31}$$

This condition can ensure that the ballistic inclination at a certain height is equal to the required ballistic inclination. Record that

$$\begin{cases} x_1 = q_L - \psi_{Mf} \\ x_2 = \dot{q}_L \end{cases} \tag{32}$$

The following equation of state can be obtained from Equations (30) and (32):

$$\begin{cases} \dot{x}_1 = x_2 \\ \dot{x}_2 = \left(\frac{\dot{V}_{ML}}{V_{ML}} - \frac{2\dot{R}_L}{R_L}\right)x_2 + \frac{\dot{R}_L}{R_L}\dot{\psi}_M \end{cases} \tag{33}$$

In order to obtain the explicit solution, it is generally assumed that when studying the guidance law, we define the following:

$$\begin{cases} \tau = -\frac{R_L}{\dot{R}_L}(R_L \neq 0) \\ \mathbf{A} = \begin{pmatrix} 0 & 1 \\ 1 & 2/\tau \end{pmatrix} \\ \mathbf{B} = \begin{pmatrix} 0 \\ 1/\tau \end{pmatrix} \\ x = (x_1, x_2)^{\mathrm{T}} \\ u = \dot{\psi}_M \end{cases} \tag{34}$$

Then, the equation of state is rewritten as follows.

$$\begin{cases} \dot{x} = \mathbf{A}x + \mathbf{B}u \\ x\left(t_f\right) = 0 \end{cases} \tag{35}$$

The selected quadratic performance index is as follows:

$$J = x^{\mathrm{T}}\left(t_f\right)\mathbf{F}x\left(t_f\right) + \frac{1}{2}\int_0^{t_f} u^2 \mathrm{d}t \tag{36}$$

where $x^T\left(t_f\right)\mathbf{F}\mathbf{x}\left(t_f\right)$ is called the compensation function and $\mathbf{F}$ is a symmetric positive semi-definite constant matrix.

According to the maximum principle, the optimal control of the quadratic performance index of the linear system is as follows.

$$u = -\mathbf{B}^{\mathrm{T}}\mathbf{P}x \tag{37}$$

The matrix **P** is derived from the inverse Riccati differential equation, and the following can be obtained by bringing it into Equation (37):

$$\dot{\psi}_M = \frac{2}{\tau}\left(q_L - \psi_{Mf}\right) + 4\dot{q}_L \tag{38}$$

By substituting Equation (38) into Equation (4),

$$-\frac{N_{MZ}g}{V_M \cos\varphi_M} = \frac{2}{\tau}\left(q_L - \psi_{Mf}\right) + 4\dot{q}_L \tag{39}$$

Then,

$$N_{MZ} = -\frac{V_M \cos\varphi_M}{g}\left[\frac{2}{\tau}\left(q_L - \psi_{Mf}\right) + 4\dot{q}_L\right] \tag{40}$$

3.3. Design of Terminal Guidance Law

The normal overload required by traditional proportional guidance when intercepting the target is directly related to the speed of the missile at the interception point and the direction of the missile's attack, and the normal overload required fluctuates greatly when the end approaches the target. Therefore, in this paper, the terminal guidance strategy is designed based on the sliding mode control theory under angle constraints and overload constraints.

(1) Longitudinal channel

For the non-linear system described by Equation (14), the system state quantity is taken as

$$X = \begin{bmatrix} R & \eta_{MH} & \eta_{TH} \end{bmatrix}^{\mathrm{T}} \tag{41}$$

By substituting into Equation (14), the following can be obtained:

$$\dot{X} = \begin{bmatrix} \dot{R} \\ \dot{\eta}_{MH} \\ \dot{\eta}_{TH} \end{bmatrix} = f + \begin{bmatrix} 0 \\ 1/V_M \\ 0 \end{bmatrix} u + \begin{bmatrix} 0 \\ 0 \\ 1/V_T \end{bmatrix} w \tag{42}$$

From Equation (42),

$$f = \begin{bmatrix} V_T \cos\eta_{TH}\cos\eta_{TL} + V_M \cos\eta_{MH}\cos\eta_{ML} \\ -\frac{V_M}{R}\sin\eta_{ML}\tan q_H\left(\cos\eta_{MH}\sin\eta_{ML} - \frac{V_T}{V_M}\cos\eta_{TH}\sin\eta_{TL}\right) - \frac{V_M}{R}\cos\eta_{ML}\left(\sin\eta_{MH} - \frac{V_T}{V_M}\sin\eta_{TH}\right) \\ -\frac{V_M}{R}\sin\eta_{TL}\tan q_H\left(\cos\eta_{MH}\sin\eta_{ML} - \frac{V_T}{V_M}\cos\eta_{TH}\sin\eta_{TL}\right) - \frac{V_M}{R}\cos\eta_{TL}\left(\sin\eta_{MH} - \frac{V_T}{V_M}\sin\eta_{TH}\right) \end{bmatrix} \tag{43}$$

The sliding mode surface is designed as follows:

$$S_{H\_ter} = \eta_{MH} - c_1\eta_{TH} \tag{44}$$

The reaching law is designed as follow:

$$\dot{S}_{H\_ter} = -\frac{c_1 N_{Y\_pre}}{V_T|S_{H\_ter}|}S_{H\_ter} - K_1\mathrm{sgn}(S_{H\_ter}) \tag{45}$$

where c_1 and K_1 are sliding mode guidance parameters, which are constants greater than 0.

Define the Lyapunov function:

$$V = \frac{1}{2}S_{H\_ter}^2 \tag{46}$$

Then,

$$\begin{aligned}\dot{V} &= S_{H\_ter}\dot{S}_{H\_ter} \\ &= S_{H\_ter}\left(-\frac{c_1 N_{Y\_pre}}{V_T|S_{H\_ter}|}S_{H\_ter} - K_1\mathrm{sgn}(S_{H\_ter})\right) \\ &= -K_1|S_{H\_ter}| - \frac{c_1 N_{Y\_pre}}{V_T|S_{H\_ter}|}S_{H\_mid}^2 < 0\end{aligned} \tag{47}$$

According to Equation (47), the designed sliding surface meets the Lyapunov stability criterion.

By substituting Equations (44) and (45) into Equation (4), the terminal guidance law of the longitudinal channel can be obtained.

$$N_{MY} = \frac{V_M}{g}\left[-(f_2 - c_1 f_2) - K_1\mathrm{sgn}(S_{H\_ter}) - \frac{c_1 N_{Y\_pre}}{V_T}\mathrm{sgn}(S_{H\_ter}) + g\cos\eta_{MH} + \frac{c_1 g}{V_T}N_{TY}\right] \tag{48}$$

(2) Lateral channel

Similarly to the longitudinal channel, the system state quantity is taken as

$$X = \begin{bmatrix} R & \eta_{ML} & \eta_{TL} \end{bmatrix}^T \tag{49}$$

By substituting into Equation (14), the following can be obtained.

$$\dot{X} = \begin{bmatrix} \dot{R} \\ \dot{\eta}_{ML} \\ \dot{\eta}_{TL} \end{bmatrix} = h + \begin{bmatrix} 0 \\ -1/(V_M\cos\eta_{MH}) \\ 0 \end{bmatrix} u + \begin{bmatrix} 0 \\ 0 \\ -1/(V_T\cos\eta_{TH}) \end{bmatrix} w \tag{50}$$

From Equation (50),

$$h = \begin{bmatrix} V_T\cos\eta_{TH}\cos\eta_{TL} + V_M\cos\eta_{MH}\cos\eta_{ML} \\ -\frac{V_M}{R\cos\eta_{TH}}\sin\eta_{MH}\cos\eta_{ML}\tan q_H\left(\cos\eta_{MH}\sin\eta_{ML} - \frac{V_T}{V_M}\cos\eta_{TH}\sin\eta_{TL}\right) - \\ \frac{V_M}{R}\left(\cos\eta_{MH}\sin\eta_{ML} - \frac{V_T}{V_M}\cos\eta_{TH}\sin\eta_{TL}\right) - \frac{V_M}{R\cos\eta_{TH}}\sin\eta_{MH}\sin\eta_{ML}\left(\sin\eta_{MH} - \frac{V_T}{V_M}\sin\eta_{TH}\right) \\ -\frac{V_M}{R\cos\eta_{TH}}\sin\eta_{TH}\cos\eta_{TL}\tan q_H\left(\cos\eta_{MH}\sin\eta_{ML} - \frac{V_T}{V_M}\cos\eta_{TH}\sin\eta_{TL}\right) - \\ \frac{V_M}{R}\left(\cos\eta_{MH}\sin\eta_{ML} - \frac{V_T}{V_M}\cos\eta_{TH}\sin\eta_{TL}\right) - \frac{V_M}{R\cos\eta_{TH}}\sin\eta_{TH}\sin\eta_{TL}\left(\sin\eta_{MH} - \frac{V_T}{V_M}\sin\eta_{TH}\right) \end{bmatrix} \tag{51}$$

The sliding mode surface is designed as follows.

$$S_{L\_ter} = \eta_{ML} - c_2\eta_{TL} \tag{52}$$

The reaching law is designed as follows.

$$\dot{S}_{L\_ter} = -\frac{c_2 N_{Z\_pre}}{V_T|S_{L\_ter}|\cos\eta_{TH}}S_{L\_ter} - K_2\mathrm{sgn}(S_{L\_ter}) \tag{53}$$

where c_2 and K_2 are sliding mode guidance parameters, which are constants greater than 0.

Define the Lyapunov function:

$$V = \frac{1}{2}S_{L\_ter}^2 \tag{54}$$

Then,

$$\begin{aligned}\dot{V} &= S_{L\_ter}\dot{S}_{L\_ter} \\ &= S_{L\_ter}\left(-\frac{c_2 N_{Z\_pre}}{V_T|S_{L\_ter}|\cos\eta_{TH}}S_{L\_ter} - K_2\mathrm{sgn}(S_{L\_ter})\right) \\ &= -K_2|S_{L\_ter}| - \frac{c_2 N_{Z\_pre}}{V_T|S_{L\_ter}|\cos\eta_{TH}}S_{L\_ter}^2 < 0\end{aligned} \tag{55}$$

According to Equation (55), the designed sliding surface meets the Lyapunov stability criterion.

By substituting Equations (52) and (53) into Equation (4), the terminal guidance law of lateral channel can be obtained.

$$N_{MZ} = \frac{V_M \cos \eta_{MH}}{g} \left[(h_2 - c_2 h_3) + K_2 \mathrm{sgn}(S_{L\_ter}) + \frac{c_2 N_{Z\_pre}}{V_T \cos \eta_{TH}} \mathrm{sgn}(S_{L\_ter}) + \frac{c_2 g}{V_T \cos \eta_{TH}} N_{YZ} \right] \quad (56)$$

4. Simulation and Analysis

The guidance strategy designed in this paper is verified and analyzed using digital simulation. Two forms of target maneuvering and non-maneuvering flight are adopted. For the non-linear missile model, the simulation is carried out according to the designed control scheme. The simulation conditions are as follows.

a. The hypersonic target flies at an altitude of 30 km at flight speed. The allowable overload is 15 g.

b. Initial conditions of the initial guidance phase: The interceptor is launched from the ground launcher at the initial speed V_{M0} = 100 m/s. The initial launch flight-path inclination is 45 degrees and the azimuth angle is −45 degrees. The engine starts for 10 s and then shuts down. The interceptor is guided near the preset turning point by the initial guidance law.

c. Initial conditions of the midcourse guidance phase: The initial flight-path inclination and azimuth angle of the midcourse guidance phase are the same as the terminal trajectory inclination and deflection angle of the initial guidance phase. The interceptor is guided near the predicted impact point by the midcourse guidance law.

d. Initial conditions of the terminal guidance phase: The initial flight-path inclination and azimuth angle of the terminal guidance phase are the same as the terminal trajectory inclination and deflection angle of the midcourse guidance phase. The interceptor is guided by the terminal guidance law to the interception point, and the intercept accuracy should be less than 10 m.

The simulation results are shown in Figures 7–15.

Figures 7 and 8 show the interceptor and target interceptor interception trajectory. When the target is non-maneuvering, the interception trajectory is ideal, and the interceptor intercepts the target successfully at 171.45 s. When the target is maneuvering, the interceptor is maneuvering with the target maneuvering. The interceptor gradually coincides with the target track in the end guidance. Finally, the target is successfully intercepted at 171.46 s. The terminal velocity of the interceptor in the initial guidance phase is 2.2 Ma, the flight-path inclination angle is 56.4 degrees, and the azimuth angle is 2.8 degrees, which is also the initial condition of the interceptor in the midcourse guidance phase. The terminal velocity of the interceptor in the midcourse guidance phase is 2.0 Ma, the flight-path inclination angle is 0.1 degrees, and the azimuth angle is −179.3 degrees, which is also the initial condition of the interceptor in the terminal guidance phase. Under the condition of target maneuvering, the terminal velocity of the interceptor in the initial guidance phase is 2.2 Ma, the trajectory tilt is 56.4 degrees, and the trajectory deflection angle is 2.8 degrees, which is also the initial condition of the interceptor in the midcourse guidance phase. The terminal velocity of the interceptor in the midcourse guidance phase is 2.0 Ma, the flight-path inclination angle is 0.1 degrees, and the azimuth angle is −179.4 degrees, which is also the initial condition of the interceptor in the terminal guidance phase.

Figures 9 and 10 show the overload of the interceptor. The maximum overload is 15 g, which is not more than the allowable overload.

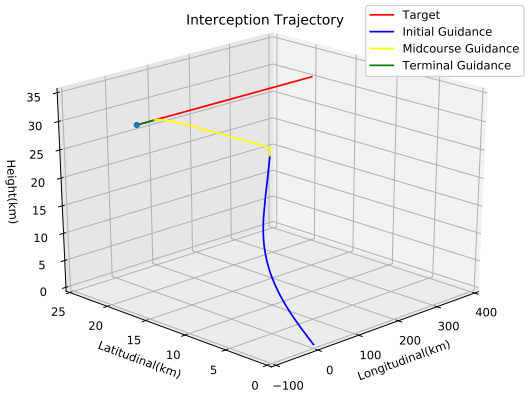

Figure 7. Interception trajectory (target non-maneuvering).

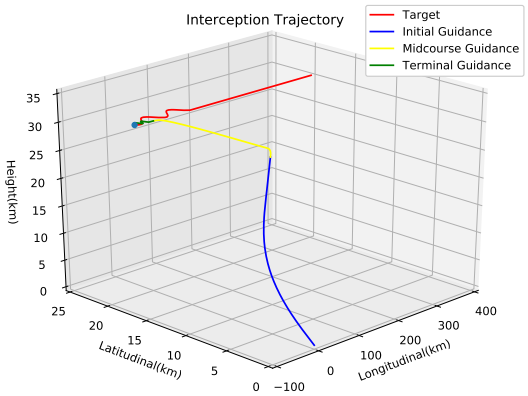

Figure 8. Interception trajectory (target maneuvering).

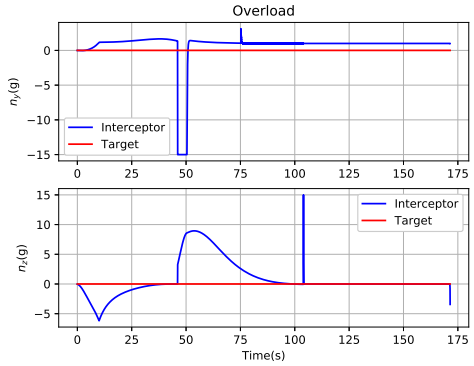

Figure 9. Overload of interceptor (target non-maneuvering).

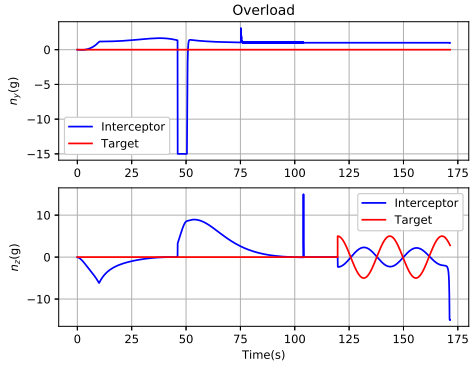

Figure 10. Overload of interceptor (target maneuvering).

Figures 11 and 12 show the trajectory tilt angle and trajectory deflection angle. When the target is non-maneuvering, the trajectory tilt angle is 0.1 degrees and the trajectory deflection angle is −179.8 degrees at the interception point. In the other case, the flight-path inclination angle angle is 0.1 degrees and azimuth angle is −167.3 degrees.

Figures 13 and 14 show the trend of line-of-sight. When the target is non-maneuvering, the line-of-sight inclination angle is 0.1 degrees, and the deflection angle is 0.3 degrees at the interception point. In the other case, the line-of-sight inclination angle is 0.1 degrees and the deflection angle is −38.6 degrees.

Figure 15 shows the Mach number of the interceptor. The Mach number increases in the first 10 s and then decreases. The Mach number is about 1.8 at the interception point.

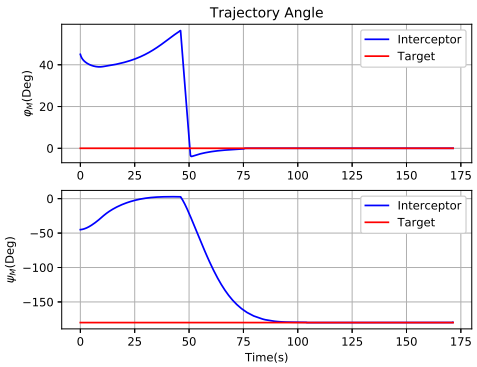

Figure 11. Trajectory angle of interceptor (target non-maneuvering).

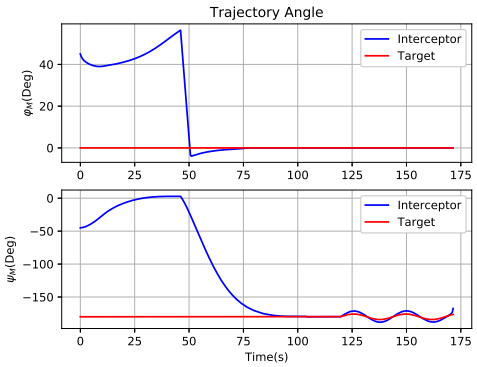

Figure 12. Trajectory angle of interceptor (target maneuvering).

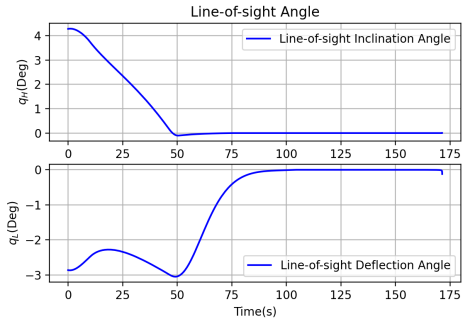

Figure 13. Line-of-sight angle (target non-maneuvering).

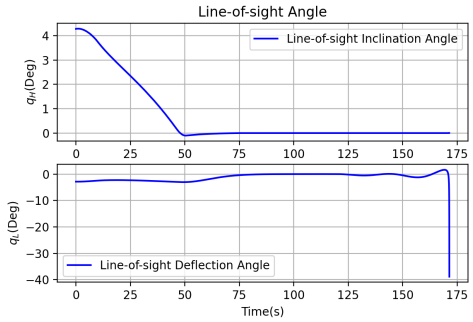

Figure 14. Line-of-sight angle (target maneuvering).

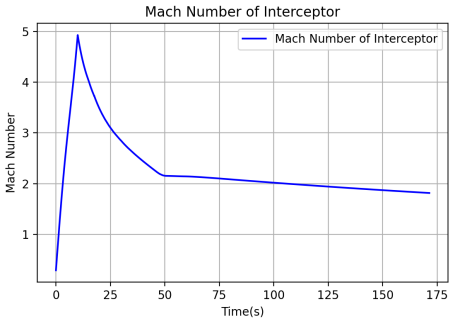

Figure 15. Mach number of interceptor.

Figures 16 and 17 show the Lyapunov functions for midcourse guidance and terminal guidance phases, respectively. It can be seen that the functions all decrease and converge to zero at the end.

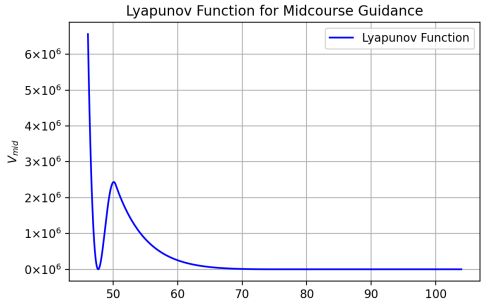

Figure 16. Lypunov functions of midcourse guidance.

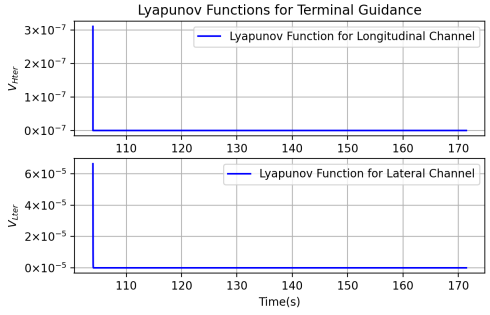

Figure 17. Lypunov functions of terminal guidance.

5. Conclusions

In this paper, we analyze the characteristics of the head pursuit interception, and a dynamic model of head pursuit interception is established. A guidance strategy is designed, and the interception process is simulated. The simulation results show that the guidance strategy designed in this paper can allow a lower-speed interceptor to intercept a higher-speed target successfully, and the interceptor can adaptively change the motion trajectory

when the target is maneuvering. To some extent, this solves the problem of high control difficulty and low guidance precision in the proportional navigation method. Using this guidance strategy, the interceptor has great robustness to acceleration interference, and the correctness of the guidance strategy is verified. The object is a hypersonic interceptor, which proves that the guidance strategy is suitable for the interception of hypersonic targets. When estimating the maneuvering acceleration of the target, the guidance strategy is shown to be suitable for the interception of complex maneuvering targets.

Author Contributions: Conceptualization, Z.L.; methodology, Z.L.; software, Z.L.; validation, Z.L. and Y.N.; formal analysis, Z.L.; investigation, Z.L.; resources, Z.L.; data curation, Y.N.; writing—original draft preparation, Z.L.; writing—review and editing, Y.N.; visualization, Z.L.; supervision, Y.N.; project administration, Y.N.; funding acquisition, Y.N. All authors have read and agreed to the published version of the manuscript.

Funding: This research was funded by Project of China Aerospace Science and Industry Corporation [No. 16510260].

Institutional Review Board Statement: Not applicable.

Informed Consent Statement: Not applicable.

Data Availability Statement: Sample data available on request.

Conflicts of Interest: The authors declare no conflict of interest. The funders had no role in the design of the study; in the collection, analyses, or interpretation of data; in the writing of the manuscript, or in the decision to publish the results.

Nomenclature

T	target
M	Interceptor
$OXYZ$	Inertial coordinate system
$OX_lY_lZ_l$	Line-of-sight coordinate system
(X_T, Y_T, Z_T)	Position of target
(X_M, Y_M, Z_M)	Position of interceptor
V_T	Velocity of target
V_M	Velocity of interceptor
A_T	Acceleration of target
A_M	Acceleration of interceptor
q_H	inclination angle of line-of-sight
q_L	deflection angle of line-of-sight
η_{TH}, η_{TL}	Attitude angle of target
η_{MH}, η_{ML}	Attitude angle of interceptor
φ_T, ψ_T	Flight-path inclination angle and azimuth angle of target
φ_M, ψ_M	Flight-path inclination angle and azimuth angle of interceptor
N_{TY}, N_{TZ}	Overload of target
N_{MY}, N_{MZ}	Overload of interceptor
R	Distance between target and interceptor
(X_{TP}, Y_{TP}, Z_{TP})	Preset turning point
S_{mid}	Sliding mode surface in midcourse guidance
$\dot{S}_{mid}$	Reaching law in midcourse guidance
S_{H_ter}, S_{L_ter}	Sliding mode surfaces in terminal guidance
$\dot{S}_{H\_ter}, \dot{S}_{L\_ter}$	Reaching laws in terminal guidance

References

1. Gollan, O.M.; Shima, T. Head Pursuit Guidance for Hypervelocity Interception. In Proceedings of the Guidance, Navigation and Control Conference and Exhibit, AIAA, Providence, RI, USA, 16–19 August 2004.
2. Gollan, O.M.; Shima. T. Precursor Interceptor Guidance Using the Sliding Mode Approach. In Proceedings of the Guidance, Navigation and Control Conference and Exhibit, AIAA, San Francisco, CA, USA, 15–18 August 2005.
3. Zhang, Y.A.; Yang, H.D.; Hu, Y.N. Modeling of Three-Dimensional Guidance Problems and Guidance Law Design Against Maneuvering Targets. *Flight Dyn.* **2005**, *21*, 41–44.
4. Zhou, X.F.; Meng, B. Virtual Target Proportional Navigation Guidance Law for Air-to-air Missile Over the shoulder. *Flight Dyn.* **2014**, *32*, 248–252.
5. Zhao, Z.H.; Shen, Y. A Head Pursuit Guidance Scheme Based on Variable Structure Control. *J. Astronaut.* **2007**, *28*, 835–839.
6. Zhou, D.; Mu, C.D.; Xu, W.L. Intelligent Adaptive Variable Structure Guidance for Space Interception. *J. Astronaut.* **1999**, *20*, 60–65.
7. Wang, J.P.; Zhou, W.W. Research on Algorithms of Midcourse Guidance Law for Head Pursuit Law. *J. Proj. Rocket. Missiles Guid.* **2013**, *33*, 37–48.
8. Guan, P.; He, Z.W.; Ge, X.S. Neural Network PID Control of Hypersonic Vehicle. *Aerosp. Control* **2018**, *36*, 8–13.
9. Ratnoo, A.; Ghose, D. Impact angle constrained interception of stationary targets. *J. Guid. Control Dyn.* **2008**, *33*, 1816–1821. [CrossRef]
10. Ratnoo, A.; Ghose, D. Impact angle constrained interception of nonstationary nonmaneuvering targets. *J. Guid. Control Dyn.* **2010**, *33*, 269–275. [CrossRef]
11. An, Z.; Xiong, F.F.; Liang, Z.N. Landing-phase guidance of rocket using bias proportional guidance and convex optimization. *Acta Aeronaut. Astronaut. Sin.* **2020**, *41*, 323606.
12. Wang, R.G.; Tang, S. Intercepting Higher-Speed Targets Using Generalized Relative Biased Proportional Navigation. *J. Northwestern Polytech. Univ.* **2019**, *37*, 682–690. [CrossRef]
13. Yan, L.; Zhao, J.G.; Shen, H.R.; Li, Y. There-dimensional united biased proportional navigation guidance law for interception of targets with angular constraints. *Acta Aeronaut. Astronaut. Sin.* **2014**, *35*, 1999–2010.
14. Mu, Z.W.; Wu, J.W.; Han, X.F. A Variable Structure Guidance Law for Bertical Attack Based on Bias Proportional Navigation. *Navig. Position. Timing* **2019**, *6*, 76–81.
15. Mu, Z.W.; Wu, J.; He, C.; Zhang, Z. New biased proportional guidance law application in air to groundcombat. *J. Command. Control* **2019**, *5*, 339–343.
16. Guo, Z. Y.; Han, Z.G. Multi-Missile Cooperative Guidance Law Design Based on Fast Non-Singular Terminal Sliding Mode. *Aero Weapon.* **2020**, *27*, 62–66.
17. Kumar, S. R.; Ghose, D. Impact time guidance for large heading errors using sliding mode control. *IEEE Trans. Aerosp. Electron. Syst.* **2015**, *51*, 3123. [CrossRef]
18. Cho, D.; Kim, H.J.; Tahk, M.J. Nonsingular sliding mode guidance for impact time control. *J. Guid. Control Dyn.* **2016**, *39*, 61. [CrossRef]
19. Hu, Q.L.; Han, T.; Xin, M. Sliding-mode impact time guidance law design for various target motions. *J. Guid. Control Dyn.* **2019**, *42*, 136. [CrossRef]
20. Si, Y.J.; Xiong, H.; Song, X.; Zong, R. Three-dimensional guidance law for cooperative operation based on adaptive terminal sliding mode. *Acta Aeronaut. Astronaut. Sin.* **2020**, *41* (Suppl. 1), 723759.
21. Yang, F.; Zhang, K. Q.; Yu, L. Adaptive second order non-singular fast terminal sliding mode guidance law. *J. Ballist.* **2020**, *32*, 7–15.
22. You, H.; Zhao, J.F.; Li, P.; Song, L.H. Second order sliding mode guidance law for nonsingular fast terminal with falling Angle constraint. *J. Proj. Rocket. Missiles Guid.* **2019**, *39*, 155–159+176.
23. Li, X. B.; Zhao, G. R.; Liu, S.; Wang, S.; Ma, L. Adaptive terminal sliding mode guidance law with impact angle and field-of-view constraints. *Control Decis.* **2020**, *35*, 2336–2344.
24. Lyu, S.; Zhu, Z. H.; Tang, S.; Yan, X. Prescribed performance slide mode guidance law with terminal line-of-sight angle constraint against maneuvering targets. *Nonlinear Dyn.* **2017**, *88*, 2101–2110. [CrossRef]
25. Harl, N.; Balakrishnan, S.N. Impact time and angle guidance with sliding mode control. *IEEE Trans. Control. Syst. Technol.* **2012**, *20*, 1436. [CrossRef]
26. Zhang, D.Y.; Lei, H.M.; Shao, L.; Li, J.; Xiao, Z.B. Interceptor trajectory programming for near space hypersonic target. *J. Natl. Univ. Def. Technol.* **2015**, *37*, 91–96.
27. Shaferman, V.; Shima, T. Cooperative Optimal Guidance Laws for Imposing a Relative Intercept Angle. *J. Guid. Control Dyn.* **2015**, *38*, 1395–1408. [CrossRef]
28. Shima, T.; Weiss, M.; Balhance, N. Cooperative Guidance Law for Intrasalvo Tracking. *J. Guid. Control Dyn.* **2017**, *40*, 1–16.
29. Shaferman, V.; Shima, T. Cooperative differential games guidance laws for imposing a relative intercept angle. *J. Guid. Control Dyn.* **2017**, *40*, 2465–2480. [CrossRef]
30. Gaudet, B.; Furfaro, R.; Linares, R. Reinforcement learning for angle-only intercept guidance of maneuvering targets. *Aerosp. Sci. Technol.* **2020**, *99*, 105746.1–105746.10. [CrossRef]

31. Li, T.; Yan, P.; Jiang, R.M.; Zhou, J. Calculation and Analysis of High-speed Missile's Aerodynamic Characteristic with Asymmetric Morphing Wings. *J. Ordnance Equip. Eng.* **2017**, *38*, 51–56.
32. Zhang, R.M.; Shi, X.T. Research on Numerical Virtual Flight of Spinning Projectile. *J. Proj. Rocket. Missiles Guid.* **2017**, 37, 117–128.
33. Ji, L.; Wu, G.D.; Wang, Z.J.; Liu, Y.K.; Xu, Y.J. Data Analysis of the Aerodynamic Characteristics of A Missile Model. *J. Proj. Rocket. Missiles Guid.* **2018**, 38, 74–78.
34. Ma, Z.Y.; Fu, Y.B.; Song, Z.C. Simulation Analysis of Missile Aerodynamic Characteristics Based on FLUENT. *Mech. Electr. Technol.* **2021**, 6, 27–30.
35. Zhu, J.Q. Research on Sliding Mode Guidance Law for Intercepting Maneuvering Targets. Master's Thesis, North University of China, Taiyuan, China, 2021.